

## Thermal to Electric Conversion with a Novel Quantum-Coupled Converter

### RLE Group

Energy Production and Conversion Group

### Sponsors

MTPV Corp

### Project Staff

P. L. Hagelstein and Dennis Wu

### Introduction

As energy prices continue to increase, technology that makes more efficient use of energy is of interest to industry and consumers. Converting heat to electricity is a potentially important capability, and technologies that can do this with high efficiency and good throughput will be very useful. In previous RLE reports, we have described a new approach to the problem that is based on quantum coupling with a cold-side single carrier converter. In this article we describe recent advances in our modeling and understanding.

The scheme is conceptually simple. In the simplest possible implementation, an electron reservoir on the cold side supplies an electron to a lower state, coupling with the hot side causes the electron to be promoted to an excited state, and then the electron proceeds to a second electron reservoir at elevated potential. An electrical load connected between the two reservoirs can be driven from the current due to the promoted electrons. Such a scheme can work with either electrons or holes (or in principle both). We have called it a single carrier converter since it is only a single carrier that is promoted at a time, as opposed to photovoltaics, in which electron-hole pairs are created.

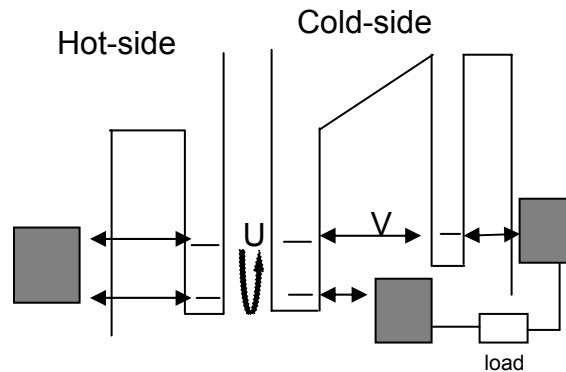


**Figure 1:** Basic Scheme. Shaded boxes indicate electron reservoirs. Arrows represent couplings. Letter U represents the electrostatic interaction while letter V represents the tunneling.

Over the past several years, we have been analyzing a specific model for the scheme that is illustrated in Figure 1. The device consists of three parts, the hot side, the cold side, and a vacuum gap in between. In this implementation, an electron is introduced into the lower level of a quantum dot, as indicated in the figure. Coulomb coupling between the electron on the cold side and a carrier on the hot side produces a quantum correlation between the cold side electron and a carrier in a quantum dot that has matched levels on the hot side, leading to excitation transfer from the hot side to the cold side. From the upper state of the quantum dot, the electron tunnels to a matched level in a second quantum dot (which provides energy selection leading to a

preferred coupling between the excited state and the second reservoir) on its way to the second reservoir which is at elevated voltage. The two cold-side reservoirs are connected to each other through an electrical load. Hence when electrons are promoted in the first quantum well, they have the possibility of tunneling to the second well and then continuing on to do electrical work before ending up in the first reservoir at ground.

### Modeling issues

Much work has gone into the development of models appropriate for this kind of device, as the analysis is complicated due to the presence of quantum coherent processes, dissipation, and constraints imposed by thermodynamics. The approach that we have found to be successful involves first defining a two-particle basis, since the cold-side electron is correlated with the hot-side carrier. We then make use of infinite-order Brillouin-Wigner theory to include dissipation as equivalent complex potentials. Finally, we view the problem in terms of a probability flow model from initial state reservoirs to final state reservoirs. In the end, we develop an expression for the current in terms of an effective coupling strength between initial and final two-particle continuum states of the form

$$\begin{aligned}
 I = & -e \int d\varepsilon_1 \int d\varepsilon_3 \int d\varepsilon_a \int d\varepsilon_b \rho_1(\varepsilon_1) \rho_3(\varepsilon_3) \rho_a(\varepsilon_a) \rho_b(\varepsilon_b) \\
 & \times \frac{2\pi}{\hbar} \left| \langle r_a, r_3 | U_{\text{eff}}(\varepsilon_1 + \varepsilon_b) | r_b, r_1 \rangle \right|^2 \delta(\varepsilon_b + \varepsilon_1 - \varepsilon_a - \varepsilon_3) \\
 & \times \left\{ p_b(\varepsilon_b) p_1(\varepsilon_1) [1 - p_a(\varepsilon_a)] [1 - p_3(\varepsilon_3)] - p_a(\varepsilon_a) p_3(\varepsilon_3) [1 - p_b(\varepsilon_b)] [1 - p_1(\varepsilon_1)] \right\}
 \end{aligned}$$

We integrate this expression over cold-side reservoir energies  $\varepsilon_1$  and  $\varepsilon_3$ , as well as hot-side reservoir energies  $\varepsilon_a$  and  $\varepsilon_b$ . The reservoir occupation probability  $p(\varepsilon)$  is taken to be equilibrium Fermi-Dirac distributions at the reservoir Fermi level. The hot-side reservoir is artificially split into two reservoirs (*a* and *b*) to make things simpler. The effective interaction between initial and final states  $U_{\text{eff}}$  is computed by developing an initial Hamiltonian in terms of two-electron basis states, using infinite-order Brillouin-Wigner theory to replace the contribution of continuum states with complex potentials, and then algebraically eliminating all states other than reservoir states.

There are technical details associated with this kind of calculation which needed to be understood before reliable estimates could be developed for specific models, and it took much time and effort for this to be accomplished. The resulting formula is deceptively simple in form in this regard.

### Results

We spent much time working with this model in order to understand both the model, and predictions from the model. Perhaps the most interesting thing about this model as describing a thermal to electric converter is that the model predicts the possibility of very efficient operation. For example, we show in Figure 2 results of ideal model (zero-loss) calculations for a set of different devices all optimized to provide a perfect match between the cold-side excited state level and the single level connected to the reservoir. One sees that the optimized efficiency at low operating voltages is roughly

$$\eta = \frac{\mu_3 - \mu_1}{\varepsilon_b - \varepsilon_a}$$

This is the difference in the cold-side reservoir Fermi levels over the difference in hot-side level energies. One can show that the incremental contribution to the current is positive as long as the Carnot limit is satisfied

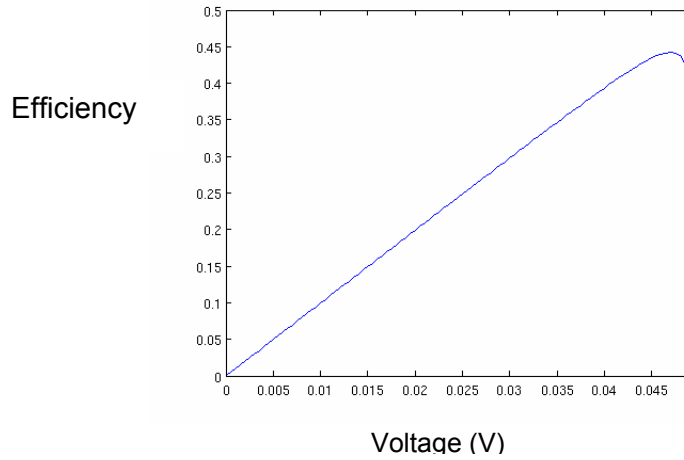


**Figure 2:** Model prediction for optimal efficiency of a set of converters optimized at the axis voltage. The hot side temperature  $T_h$  is 600 K, and the cold side temperature  $T_c$  is 300 K.

$$\frac{\mu_3 - \mu_1}{\mathcal{E}_b - \mathcal{E}_a} < \frac{T_h - T_c}{T_h}$$

The device is capable, according to this modeling, of operation up close to the Carnot limit. The associated converted power approaches zero at the Carnot limit, so that there is no chance of finite conversion at the Carnot limit. The maximum load power is obtained near 65% of the Carnot limit.

The model is most sensitive to loss of the excited state of the two-level quantum dot on the cold side. To study this, we have examined the optimum efficiency of a set of devices in which we allow the excited state to decay with various rates. The results are illustrated in Figure 3. One sees that the efficiency is rapidly degraded with increasing loss rate.

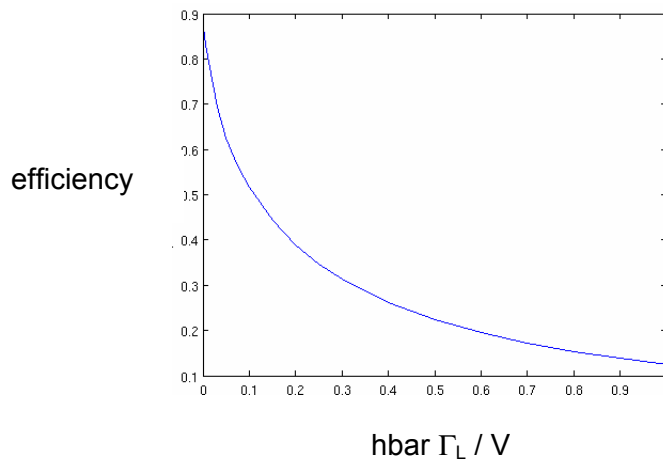


**Figure 3:** Model prediction for optimal efficiency of a set of converters as a function of the loss rate  $\Gamma_L$  of the excited state of the cold-side quantum dot. The hot-side temperature  $T_h$  is 600 K, and the cold side temperature  $T_c$  is 300 K. Here  $V$  is the tunneling rate from the state.

### Hot side with surface image charges

A drawback of the model discussed above is that the hot-side levels and cold-side levels are entangled, so that the optimum performance is obtained under conditions where the quantum coupling strength  $U$  is about twice  $V$ , and the relaxation times for both cold-side and hot-side levels (other than the cold-side excited state of the quantum dot) are matched. This becomes a drawback since it is difficult to arrange for the coupling strength  $U$  to be sufficiently large so that the load power is large enough to be of interest. Designs which satisfy this in the case of an implementation based on alloys near InSb have quantum dots that are separated by tens of Angstroms, which is not practical with current technology.

Consequently, we have been seeking modifications of the scheme which would decouple the hot side from the cold side in terms of design constraints. For example, if the coupling strength  $U$  is much less than the tunneling matrix element  $V$ , then the current scales as  $U^2$ . If the relaxation time of the hot side is very fast, then the hot side looks incoherent, and the scaling is also like  $U^2$ . In either case, the hot side decouples from the cold side in this limit to some degree, and we can think of the combined hot and cold system as behaving more like our intuition would suggest. In this case, if we couple to many dipoles on the hot side, we expect their contributions to add linearly.

We developed models for coupled between the cold side converter, and various hot side models with distributions of dipoles. We found (as expected) that we could develop expression for coupling in terms of real and imaginary parts of dielectric constants (or real dielectric constants and conductivities). Model results for these systems were not overly encouraging, as the associated load power was computed to be relatively small. At some point, the question came up of how to model conductors which have free charges and develop surface image charges. After thinking about the problem for a while, it became clear that charge movement in the quantum dot would promote movement in the image charge on a nearby conductive surface. The movement of the image charge would constitute a surface current, and associated resistive loss as well. Such power dissipation, which could be estimated classically, would provide the rate at which power is dissipated in the hot side by the return current of the cold side converter. If one could develop an associated quantum mechanical model for this dissipation, then detailed balance could be used to estimate the forward rates and device efficiency.

To model image charge physics correctly would require implementing a rather sophisticated model with many states, and correspondingly a long development time. However, it is possible to specify a much simpler two-level system model with the same dynamics as the image charge, and hence the same classical power dissipation. The resulting two-level model involves degenerate levels, but otherwise fits into the framework of the model discussed above, and we are able to develop model calculations for this kind of scheme. What is interesting is that the equivalent coupling strength is quite large, and independent of the gap thickness, at least in the limit that the system is electroquasistatic.

The scheme that results is much simpler than what is required if one were to try to juxtapose two very small quantum dots, had we sought to actually implement the hot side using a quantum dot. A schematic of converter next to a hot metal surface is illustrated in Figure 4. In this case the hot side can be a simple flat surface of a metal, semi-metal, or highly doped semiconductor. Across the gap, the cold-side has two quantum dots on the surface. Dot 1 has two levels and they couple to the hot-side dipole via Coulomb interaction. Dot 2 has one level and it couples to the excited level of dot 1 through tunneling. The lower level of dot 1 relaxes to reservoir 1, which is at ground voltage. The dot 2 level relaxes to reservoir 2 which is at an elevated voltage. Reservoir 1 has a branch off the bus in order to couple the lower level of dot 1. The branch is horizontal to dot 1 and it faces the center of dot 1 with a distance. Reservoir 2 is parallel to dot 1 and it runs on the surface next to dot 2 with a distance. The cold-side structure is repeated over the surface with the reservoir 1 buses linked together and the reservoir 2 buses linked together. Reservoir 1 and reservoir 2 are connected through the load.

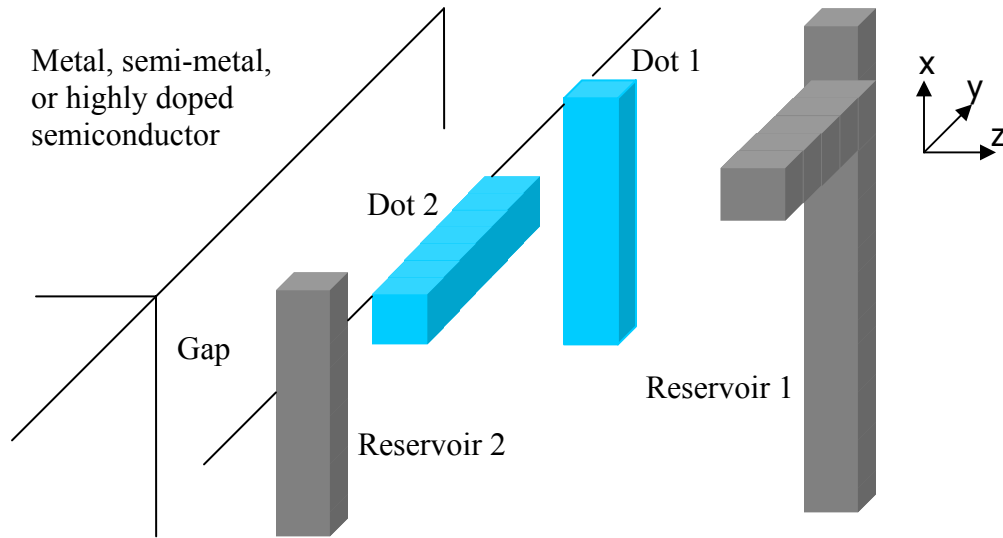


**Figure 4:** An example implementation of one unit of the device. Dot 1 holds two levels and dot 2 holds one level. The dots are presumed to be implemented in a substrate that is not shown. Reservoir 1 is at ground while reservoir 2 is at an elevated voltage. The unit is repeated over a larger area with common reservoirs 1 and 2.

### Model results

We present a specific design of this implementation and the associated simulation results. The temperature on the hot-side is 1300K and that on the cold-side is 300K. Dot 1 has  $x \times y \times z$  dimension  $(95 \text{ \AA}) \times (60 \text{ \AA}) \times (60 \text{ \AA})$  and is implemented using InAs. The energy separation of the dot 1 levels is 0.2 eV. Both reservoir 1 and reservoir 2 are made up of n-type InSb doped such that its relaxation time at 0.2 eV is 0.1 ps. With sufficient coupling to the reservoirs, the relaxation time of the lower level of dot 1 to reservoir 1 is 0.1 ps, as is the relaxation time of the single level in dot 2 to reservoir 2. The hot-side is metallic iron, of which relaxation time at 1300 K is 0.29 fs. Dot 2 is assumed to be InAs, with dimensions  $(40 \text{ \AA}) \times (65 \text{ \AA}) \times (70 \text{ \AA})$ , and is horizontally pointing to the top part of dot 1. Dot 2 holds a level that is lower than the excited level of dot 1 by 137 mV such that at a voltage of 137 mV they become resonant. Note that Figure 4 is not drawn to scale. The distance between dot 1 and dot 2 is 25 Å. Reservoir 1 branch is horizontally positioned 50 Å away from the center of dot 1. Due to this spatial orientation, reservoir 1 coupling to the excited level of dot 1 is small and the relaxation time of this excited level is basically the bulk pure InAs relaxation time 1.2 ps. Reservoir 2 is located 25 Å next to dot 2. The surrounding material on the cold-side is GaAs.

The electrostatic interaction between the surface charges and the cold-side dipole is independent of the vacuum gap thickness. However, for thicknesses greater than the wavelength associated with the transition energy of the dot 1 levels divided by  $2\pi$ , the effects of transverse photons may degrade device performance. The absorption wavelength corresponding to 0.2 eV is  $6.2 \mu\text{m}$ , and hence the gap should be below  $1 \mu\text{m}$  in this case.

Shown in Figure 5 and Figure 6 are the power on load density and efficiency as a function of voltage for the device. We have made the assumption that each device unit occupies an area of  $(1000 \text{ \AA}) \times (1000 \text{ \AA}) = 10^{-10} \text{ m}^2$ . The maximum efficiency 57% occurs at voltage 137 mV and the corresponding power on load density is  $702 \text{ W/cm}^2$ .

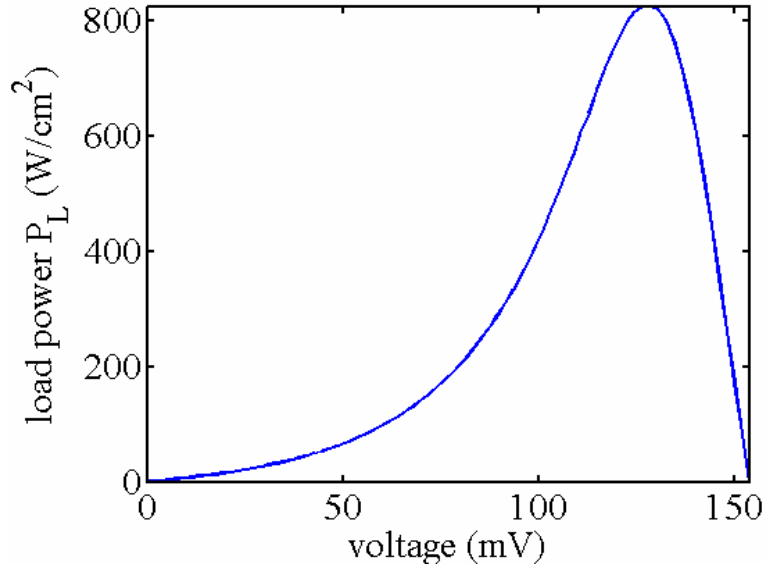


**Figure 5:** load power density as a function of voltage for a hot-side iron design operating at 0.2 eV, with the assumption of  $1000 \text{ \AA} \times 1000 \text{ \AA}$  device unit area

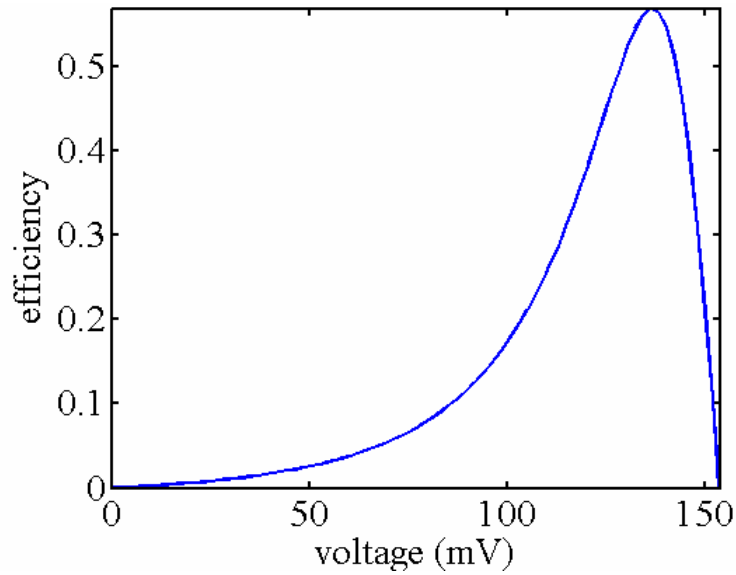


**Figure 6:** Efficiency as a function of voltage for a hot-side iron design operating at 0.2 eV, with the assumption of  $1000 \text{ \AA} \times 1000 \text{ \AA}$  device unit area

## Nuclear reaction matrix elements including phonon coupling

### RLE Group

Energy Production and Conversion Group

### Sponsors

Bose foundation, Griswold gift fund, Kimmel gift fund, and Darpa

### Project Staff

Irfan Chaudhary and Peter L. Hagelstein

### Introduction

In nuclear physics, the vacuum approximation has long been used as a tool in the analysis of nuclear reactions. The basic idea is that in a collision between two nuclei, nothing happens until the nuclei get close enough for the strong force to play a role, and when this happens the reaction dynamics takes place locally on a time scale short enough that there is not enough time to communicate to neighboring atoms that a reaction has occurred. Hence, the answer that one gets for a vacuum calculation by all rights should be the same as if one had included the local environment on the atomic scale in the problem.

However, since 1989 there have been reported many experiments involving metal deuterides in which anomalies (such as excess heat, correlation between heat and  $^4\text{He}$ , as well as other effects) appear. These effects are not consistent with the nuclear reaction physics according to the vacuum approximation, and they provide us with motivation for exploring coupling between nuclear reactions and the local environment, as well as the consequences of such coupling. Given that the nuclear center of mass coordinate in a solid is a phonon operator, it follows most naturally to examine the coupling between nuclear reactions and phonon modes. We have recently developed a model for incorporating phonon exchange in strong force matrix elements of the type that appear in simple reaction calculations in a Born type of approximation. This enables a direct calculation of how many phonons are exchanged in the course of a reaction (at least in a Born approximation), as well as the associated angular momentum exchange. The ability to perform such calculations lies at the basis of the analysis of proposed models for reaction mechanisms relevant to the anomalies.

### Connection with conventional phonon exchange models

Phonon exchange with electrons is known in the solid state and chemical physics literature. In the solid state literature, phonon exchange with electrons can be derived from the Coulomb interaction in the form

$$\hat{V} = - \sum_{i,j} \frac{Z_j e^2}{4\pi\epsilon_0 |\hat{\mathbf{R}}_j - \mathbf{x}_i|}$$

In this case, the nuclear center of mass coordinate  $\hat{\mathbf{R}}_j$  is a phonon operator. One sees here the basic Coulomb interaction, with the distance between the electron ( $\mathbf{x}_i$ ) and nucleus depending on the phonon excitation. In the event that the electron and phonon wavefunctions separate, an associated matrix element can be written as

$$M_{fi} = - \left\langle \Psi_f^L(\mathbf{q}) \psi_f(\mathbf{x}_1 \cdots \mathbf{x}_n) \left| \sum_{i,j} \frac{Z_j e^2}{4\pi\epsilon_0 |\hat{\mathbf{R}}_j(\mathbf{q}) - \mathbf{x}_i|} \right| \Psi_i^L(\mathbf{q}) \psi_i(\mathbf{x}_1 \cdots \mathbf{x}_n) \right\rangle$$

This constitutes a simple formula from which electron-phonon interactions might be developed from first principles. Similarly, in the case of neutron scattering, the inclusion of phonon interaction can be accomplished similarly. In this case, an idealized potential of the form

$$\hat{V} = V_0 \sum_{i,j} \delta^3(\hat{\mathbf{R}}_j - \mathbf{r}_i)$$

Once again, what matters is the separation between the neutron ( $\mathbf{r}_i$ ) and the nuclear center of mass ( $\hat{\mathbf{R}}_j$ ), the latter which is made up of phonon amplitude operators. An interaction matrix element can be written in the case of a separable wavefunction

$$M_{fi} = \left\langle \Psi_f^L(\mathbf{q}) \psi_f(\mathbf{r}) \left| \sum_{i,j} V_0 \delta^3(\hat{\mathbf{R}}_i(\mathbf{q}) - \mathbf{r}_j) \right| \Psi_i^L(\mathbf{q}) \psi_i(\mathbf{r}) \right\rangle$$

The coupling between neutron and phonons is made clear in this interaction matrix element.

### Simplified interaction matrix element for a nuclear reaction

The extension of the approach to the case of nuclear reactions is in principle straightforward. For example, if we adopt an idealized scalar nuclear potential model

$$\hat{V} = \sum_{\alpha < \beta} v_n(\mathbf{r}_\alpha - \mathbf{r}_\beta)$$

in terms of nucleon (that is, proton or neutron) coordinates ( $\mathbf{r}_\alpha, \mathbf{r}_\beta$ ), then the interaction matrix element written also in terms of nucleon coordinates is

$$M_{fi} = \left\langle \Psi_f^L(\mathbf{r}_1 \cdots \mathbf{r}_n) \left| \sum_{\alpha, \beta} v_n(\mathbf{r}_\alpha - \mathbf{r}_\beta) \right| \Psi_i^L(\mathbf{r}_1 \cdots \mathbf{r}_n) \right\rangle$$

Since the strong force interaction in a nuclear reaction is written in terms of a potential between individual nucleons, the matrix element appears simplest when written in terms of nucleon coordinates. However, we would like to express the matrix element in terms of phonon coordinates, and not nucleon coordinates. As an intermediate step, we might express it in terms of nuclear center of mass coordinates ( $\mathbf{R}$ ), and relative nucleon coordinates ( $\xi$ ).

$$M_{fi} = \int \Psi_f^L(\{\mathbf{R}^f\}, \{\xi^f\}) \sum_{\alpha < \beta} v_n(\mathbf{r}_\alpha - \mathbf{r}_\beta) \Psi_i^L(\{\mathbf{R}^i\}, \{\xi^i\}) \\ \times \prod_{\alpha} \delta^3(\mathbf{r}_\alpha^f - \mathbf{r}_\alpha^i) d\{\xi^i\} d\{\xi^f\} d\{\mathbf{R}^i\} d\{\mathbf{R}^f\}$$

The form of this interaction matrix element appears a bit complicated since there are initial state center of mass and relative coordinates, as well as final state coordinates. This is necessary since some of the nuclei in the final state lattice may be different than the nuclei in the initial state lattice, since a nuclear reaction may have taken place. Once the lattice has been specified in terms of center of mass coordinates, then it is straightforward to convert to phonon coordinates. We may write

$$M_{fi} = \int \Psi_f^L(\mathbf{q}^f, \{\xi^f\}) \sum_{\alpha < \beta} v_n(\mathbf{r}_\alpha - \mathbf{r}_\beta) \Psi_i^L(\mathbf{q}^i, \{\xi^i\}) \prod_{\alpha} \delta^3(\mathbf{r}_\alpha^f - \mathbf{r}_\alpha^i) d\{\xi^i\} d\{\xi^f\} d\mathbf{q}^i d\mathbf{q}^f$$

If the phonon coordinates and internal nuclear coordinates separate (which should be quite a good approximation), then it is possible to recast this matrix element in the form

$$M_{fi} = \int \Psi_f^L(\mathbf{q}^f) \hat{v}(\mathbf{q}^f, \mathbf{q}^i) \Psi_i^L(\mathbf{q}^i) \delta^N(\mathbf{q}^f - \mathbf{A}\mathbf{q}^i - \mathbf{b}) d\mathbf{q}^i d\mathbf{q}^f$$

In this matrix element, the effective potential operator is developed over an appropriate integration over internal relative coordinates. Such a matrix element is sometimes written more simply as

$$M_{fi} = \int \Psi_f^L(\mathbf{q}^f) \hat{v}(\mathbf{q}^f, \mathbf{q}^i) \Psi_i^L(\mathbf{q}^i) d\mathbf{q}^i$$

where the final state phonon mode amplitudes are in general related to the initial amplitudes through a rotation and translation

$$\mathbf{q}^f = \mathbf{A}\mathbf{q}^i + \mathbf{b}$$

We see that in the case of a much simplified model nuclear potential, the inclusion of phonon exchange in a nuclear reaction matrix element is straightforward, and fits generally within standard theory for phonon exchange.

### Phonon exchange in the case of realistic nuclear potentials

We benefited in the formulation above from the use of a simple nuclear potential model. However, such simplified nuclear potential models do not give a good description of a nuclear reaction. Instead, one needs to use a more realistic nuclear potential, which will depend on spin and isospin. In this case, we can make progress by adopting nuclear wavefunctions of the form

$$\Psi = \sum_j C_j R_j(\{\mathbf{r}\}) S_j(\{\sigma\}) T_j(\{\tau\})$$

Since we choose to work with nuclear wavefunctions that are antisymmetric, this kind of construction must be carried out using basis vectors of operators that are representations of the symmetric group. Once this construction is made, then the evaluation of the nuclear matrix element is straightforward. For example, we may develop an interaction matrix element generally in the vacuum case in terms of spatial coordinates

$$\left\langle \Psi' \left| \sum_{\alpha < \beta} V(\alpha, \beta) \right| \Psi \right\rangle = \sum_{j,k} \left\langle R'_k(\{\mathbf{r}\}) \left| V_R^{k,j}(\{\mathbf{r}\}) \right| R_j(\{\mathbf{r}\}) \right\rangle$$

Here, we have included the spin and isospin algebra in the definition of the effective interaction potential

$$V_R^{k,j}(\{\mathbf{r}\}) = C_k^* C_j \left\langle S'_k(\{\sigma\}) T'_k(\{\tau\}) \left| \sum_{\alpha < \beta} V(\alpha, \beta) \right| S_j(\{\sigma\}) T_j(\{\tau\}) \right\rangle$$

By making use of this kind of construction, we have succeeded in making the calculation with the realistic nuclear potential look like a summation over terms each of which is of the form given above. This is both interesting and practical. The lattice can be included simply by introducing the nuclear center of mass coordinates of the nonreacting nuclei as spectators in the wavefunctions, and repeating the calculation.

### Phonon exchange in the case of a realistic nuclear potential

We considered in detail such a calculation. The initial state contains two deuterons, and the final state contains a neutron and a  $^3\text{He}$  nucleus, and we chose as a model realistic nuclear potential the Hamada-Johnston potential. The interaction matrix element can be expressed as a sum of integrals, one of which we discuss here. The integral of interest that we focused on can be written as

$$I = \int \Psi_f^L(\mathbf{q}^f, \mathbf{r}_4^f) \hat{v}(\mathbf{q}^f, \mathbf{q}^i) \Psi_i^L(\mathbf{q}^i, \mathbf{r}_{dd}^i) \delta^{N_q}(\mathbf{q}^f - \mathbf{A}\mathbf{q}^i - \mathbf{b}) d\mathbf{r}_4^f d\mathbf{r}_{dd}^i d\mathbf{q}^i d\mathbf{q}^f$$

Here the final state contains a neutron ( $\mathbf{r}_4^f$ ) in addition to the lattice, and the initial state contains a description of the two deuterons as looking like a  $^4\text{He}$  to the lattice, with the relative separation between the deuterons ( $\mathbf{r}_{dd}^i$ ) included separately. The effective interaction in this case is

$$\begin{aligned} \hat{v}(\mathbf{q}^f, \mathbf{q}^i) &= \int \phi_{3\text{He}}(\xi_{32}^f, \xi_{21}^f) V(\xi_{21}^f) \phi_d(\xi_{21}^i) \phi_d(\xi_{43}^i) \\ &\times \delta^3\left(\left(\mathbf{R}_{3\text{He}}^f(\mathbf{q}^f) - \frac{1}{3}\xi_{32}^f - \frac{2}{3}\xi_{21}^f\right) - \left(\mathbf{R}_{4\text{He}}^i(\mathbf{q}^i) - \frac{1}{2}\xi_{21}^i - \frac{1}{2}\xi_{43}^i\right)\right) \\ &\times \delta^3\left(\left(\mathbf{R}_{3\text{He}}^f(\mathbf{q}^f) - \frac{1}{3}\xi_{32}^f + \frac{1}{3}\xi_{21}^f\right) - \left(\mathbf{R}_{4\text{He}}^i(\mathbf{q}^i) + \frac{1}{2}\xi_{21}^i - \frac{1}{2}\mathbf{r}_{dd}^i\right)\right) \\ &\times \delta^3\left(\left(\mathbf{R}_{3\text{He}}^f(\mathbf{q}^f) + \frac{2}{3}\xi_{32}^f + \frac{1}{3}\xi_{21}^f\right) - \left(\mathbf{R}_{4\text{He}}^i(\mathbf{q}^i) - \frac{1}{2}\xi_{21}^i - \frac{1}{2}\mathbf{r}_{dd}^i\right)\right) \\ &\times \delta^3\left(\mathbf{r}_4^f - \left(\mathbf{R}_{4\text{He}}^i(\mathbf{q}^i) + \frac{1}{2}\xi_{21}^i + \frac{1}{2}\mathbf{r}_{dd}^i\right)\right) d\xi_{21}^f d\xi_{32}^f d\xi_{21}^i d\xi_{43}^i \end{aligned}$$

For the specific spin and isospin channels that we selected, the Hamada-Johnston potential leads to an effective potential of the form

$$V(\mathbf{r}) = 18\sqrt{3} \frac{(x+iy)z}{r^2} y_T^{et}(\mu r) + \sqrt{3} (\hat{L}_+ \hat{L}_z + \hat{L}_z \hat{L}_+) y_{LL}^{et}(\mu r)$$

### Discussion

The calculation of nuclear matrix elements is complicated by the fact that empirical nuclear potentials have terms that depend on space, spin, and isospin, and require nuclear wavefunctions that have well defined symmetries in space, spin, and isospin. In order to include phonon exchange, we needed to develop wavefunctions with specific spin and isospin parts (which are themselves basis vectors of operators that are representations of the symmetric group) and general spatial dependence (consistent with symmetric group properties). Once we use such wavefunctions, the calculations are straightforward. Although such a model and calculation might be viewed as being completely standard, we have so far found only one reasonably obscure paper from the 1960s in the nuclear physics literature discussing the use of this kind of wavefunction construction for the vacuum case.

**References**

1. I. Chaudhary and P. L. Hagelstein, "Few-body nuclear wavefunctions," *Proceedings of the 10<sup>th</sup> International Conference on Cold Fusion*, Cambridge, MA, Aug. 2003, p. 887.
2. I. Chaudhary and P. L. Hagelstein, "Four-body RST general nuclear wavefunctions and matrix elements," *Proceedings of the 12<sup>th</sup> International Conference on Cold Fusion*, Yokohama, Japan, Dec. 2005, (in press).
3. I. Chaudhary and P. L. Hagelstein, "Inclusion of phonon exchange in a nuclear reaction matrix element," submitted to *Phys. Rev. B*. Available on the web at arXiv:cond-mat/0606585

## Simple model for excess heat in metal deuterides

### RLE Group

Energy Production and Conversion Group

### Sponsors

Spindletop Corporation

### Project Staff

Peter L. Hagelstein

### Introduction

Following the initial report of the appearance of an excess heat effect in metal deuterides in 1989, we were motivated to explore physical mechanisms in the hope of developing theoretical models that could provide insight and predictive capability. The development of even the simplest models has as a prerequisite the development of an underlying physical picture which is relevant. So, over the years, experimental results have shed more light on things and our physical understanding has improved, and this had led to the recent development of some very simple models which appear to relevant to excess heat production. We will discuss these models and associated ideas in what follows.

### Equivalent two-level systems and excitation transfer

We discussed phonon exchange in connection with an interaction matrix element for a nuclear reaction in a separate article in this report. Reactions at different sites that couple to a common highly excited phonon mode have the possibility of being coupled together, which can give rise to qualitatively new physics. And if a reaction at one site can couple to a reaction at a second, there is no reason that reactions at other sites can do so as well. Very quickly, we end up with many site models in which excitation is being transferred from one set of levels to another set.

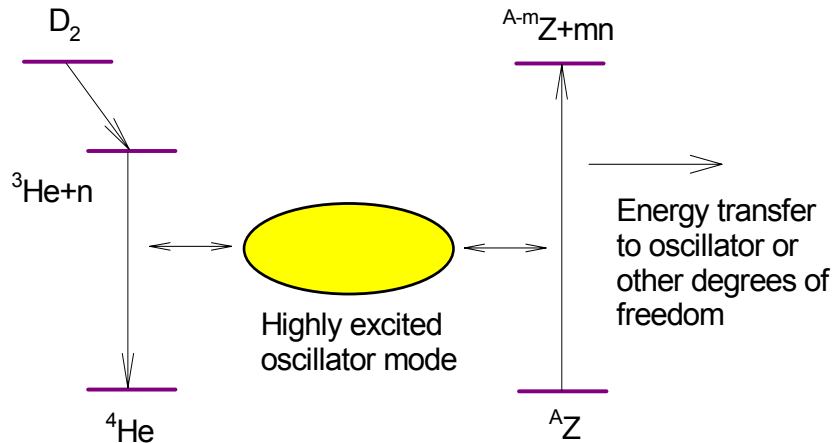


**Figure 1:** Schematic of excitation transfer scheme. The transition energy for  $D_2$  (through  ${}^3\text{He}+n$  intermediate states) to  ${}^4\text{He}$  is transferred to other nuclei, producing a neutral plus daughter excited state, mediated by coupling to a highly excited phonon mode or other macroscopic degree of freedom.

Such models rapidly become too complicated to analyze in detail, which motivates us to find simpler idealized models which we can analyze that work the same way. Perhaps the simplest way to develop such reduced models is to make use of equivalent two-level systems. For example, molecular deuterium embedded in a condensed matter environment can serve as the

upper state of such a two-level system, and  $^4\text{He}$  can be the ground state. If the excitation is transferred to neutral plus daughter states in Pd (or in other nuclei), then the ground state nuclei can be carried over to be the ground state of a second two-level system, and the neutral plus daughter can serve as the upper state. This is depicted in Figure 1.

Excitation transfer can only work if both transitions are coupled to a common highly excited phonon mode. This coupling is very weak since it involves a tunneling matrix element for tunneling through a Coulomb barrier from atomic scale separation to nuclear scale separation. Not much energy is exchanged with the phonon mode in association with this excitation transfer. On the receiver side, the excited neutral plus daughter states are able to transfer their excitation rapidly from site to site, exchanging a small amount of excitation in association with each transfer. We have constructed many-site models that describe this kind of dynamics, but we do not as yet have satisfactory solutions in general. However, we have proposed a further simplification that appears to yield models that we can analyze.

### Excitation transfer between Dicke systems

On the receiver side, we can think of the many-site model in terms of a set of two-level systems that are coupled to a highly excited oscillator. In the case of linear coupling, this kind of system is discussed in the literature in terms of coupled Dicke and SHO systems, or more simply as the spin-boson problem. In our system, the coupling must be nonlinear, but this is thought not to change the problem very much. Mixing between the Dicke system and oscillator produces a hybrid mixed system that has a great many levels that are roughly equi-spaced at the oscillator energy. Transferring excitation to this system can be thought of schematically as illustrated in Figure 2.

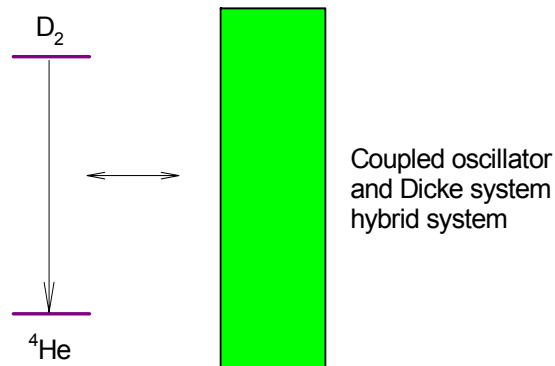


**Figure 2:** Simplification of scheme illustrated above. The receiver-side nuclei and oscillator are strongly coupled, so we think of the model in terms of a two-level system weakly coupled to a hybrid Dicke and oscillator system.

We have studied the coupled oscillator and Dicke system both analytically and numerically, as discussed briefly in the ICCF12 proceedings. These studies have pointed to the possibility of a simpler kind of model which is easier to understand.

In the simplest view of the problem, excitation is transferred slowly from the  $D_2/{}^4\text{He}$  Dicke system to the receiver nuclei Dicke system, and then lost through coupling to the phonon mode. The initial excitation transfer is very slow, because it is hindered due to tunneling through the Coulomb barrier. The rapid excitation transfer between the receiver nuclei doesn't accomplish much (other than stabilization of the excited states) on a short time scale. On a longer time scale, the rapid excitation transfer leads to net de-excitation of excited states and net transfer of energy to the oscillator. Consequently, it seems plausible to examine models in which the excitation transfer between Dicke systems is modeled in detail, and with the excitation loss on the receiver side

added separately. One way to do this is to study a model for resonant excitation transfer between weakly coupled Dicke systems, which is governed by the Hamiltonian

$$H = \frac{\Delta E}{\hbar} \hat{S}_z^1 + \frac{\Delta E}{\hbar} \hat{S}_z^2 + \frac{V}{\hbar^2} e^{-G} \left( \hat{S}_+^1 \hat{S}_-^2 + \hat{S}_-^1 \hat{S}_+^2 \right)$$

Results from simulations of the dynamics of the excitation transfer are shown in Figure 3. One sees in these results that the excitation is initially localized in the upper state of the  $D_2/{}^4\text{He}$  system, and then is transferred to the receiver nuclei. The associated rate is initially low, and then increases rapidly, so that most of the excitation transfer happens in a “burst”.

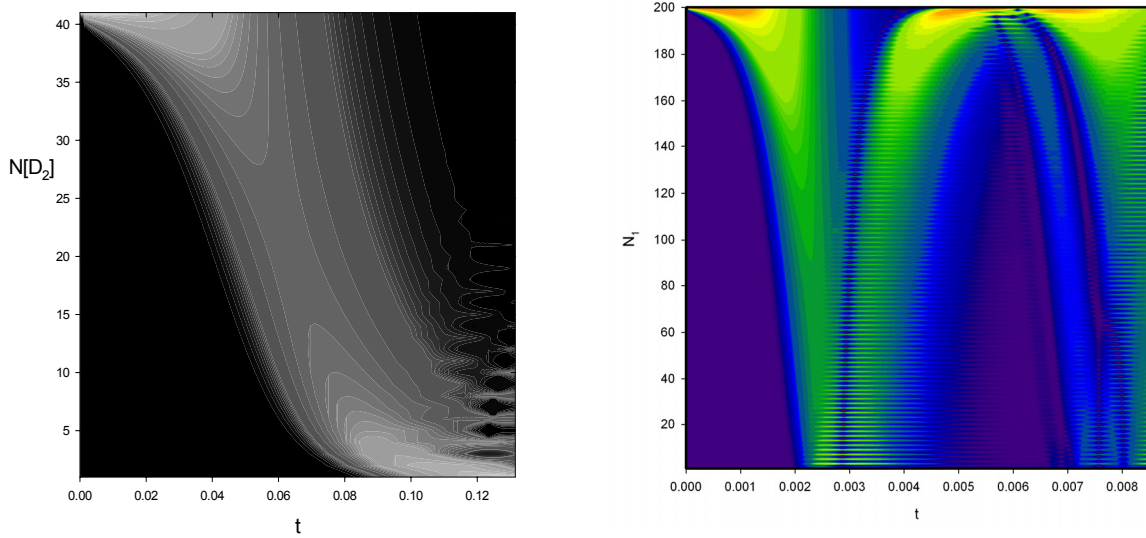


**Figure 3:** Simulation results for excitation transfer for resonant Dicke systems. Shown is the logarithm of the  $D_2$  population distribution as a function of time for: the case of a balanced system in which 40 two-level systems initially excited is coupled to 40 two-level systems initially in the ground state (left); and the case of an unbalanced system in which 200 two-level systems initially excited are coupled to a large number of two-level systems initially in the ground state.

It is possible to use Ehrenfest's theorem to develop evolution equations for the expectation value of the populations. Doing so leads to coupled second-order differential equations for the upper state populations of the two systems

$$\begin{aligned} \frac{d}{dt} n_1 &= v_1 & \frac{d}{dt} n_2 &= v_2 \\ \frac{d}{dt} v_1 &= a & \frac{d}{dt} v_2 &= -a \end{aligned}$$

$$a = \frac{2V^2 e^{-2G}}{\hbar^2} \left\{ [N_1 - n_1][N_2 - n_2][n_2 - n_1] + n_1 n_2 [N_1 - n_1 - N_2 + n_2] + [N_1 - n_1] n_2 - [N_2 - n_2] n_1 \right\}$$

However, this does not include the loss of population on the receiver side. The receiver side loss in the model under discussion is coherent, at least in the limit that the oscillator does not lose phase coherence. To include such loss correctly requires the development of more sophisticated

models, which has not yet been done. Nevertheless, we can develop an incoherent loss model simply by augmenting the evolution equations with receiver-side relaxation. This leads to

$$\begin{aligned} \frac{d}{dt}n_1 &= v_1 & \frac{d}{dt}n_2 + \frac{n_2}{T} &= v_2 \\ \frac{d}{dt}v_1 + \frac{v_1}{T} &= a & \frac{d}{dt}v_2 + \frac{v_2}{T} &= -a \end{aligned}$$

The resulting equations give solutions that describe excess heat bursts.

### Excess heat burst model for the Fleischmann-Pons experiment

We can use this model to develop predictions for excess heat bursts in Fleischmann-Pons experiments. Such an exercise is interesting, since we can check to see whether such a model is relevant. On the one hand, the model describes coupled resonant Dicke systems with empirical loss, which may be what the important physics in the experiment is. On the other hand, the model describes coupling between a fixed number of  $D_2/{}^4He$  systems and receiver nuclei, which is probably not a good approximation since  $D_2$  and  ${}^4He$  are mobile. In addition, the highest power is obtained in the model when the relaxation time is matched to the coherent transfer rate, which provides the best match with experiment. We would prefer to use an independent estimate for the relaxation time. Although we now have first generation models to work with for such comparisons, at this point it seems to make the most sense to work with an empirical relaxation time.

Given this discussion, we have assembled a set of input parameters which leads to predictions which resemble a typical excess heat burst from a Fleischmann-Pons cell (see Table 1).

Parameter	value
$e^{-G}$	$1.7 \times 10^{-36}$
$\sqrt{v_{nuc} / v_{mol}}$	$8.5 \times 10^{-8}$
$U_{DD}$	3 MeV
$\Delta r$	$10 \mu m$
$f_{DD}$	$1.5 \times 10^{-4}$
$N_{DD}$	$5.6 \times 10^{15}$
$N_{4He}$	$3.8 \times 10^{10}$
$N_{rec}$	$2.3 \times 10^{19}$
$\Omega$	$2.4 \times 10^{-4} \text{ sec}^{-1}$
$E_{tot}$	21.6 kJ

**Table 1:** Parameters used for standard Fleischmann-Pons excess heat pulse.

In this table we have defined  $\Omega$  according to

$$\Omega = \sqrt{N_{DD}N_{rec}} \frac{V e^{-G}}{\hbar}$$

where

$$V = \sqrt{\frac{v_{nuc}}{v_{mol}} U_{DD}}$$

The two deuterons are initially localized in a molecular volume  $v_{mol}$  associated with  $D_2$  in the initial state, and are localized in a nuclear volume  $v_{nuc}$  in the final state. In addition to overcoming the Coulomb barrier, the two deuterons must overcome a volume change as well. The relaxation time is taken such that  $\Omega T$  is unity (in many Fleischmann-Pons experiments, conditions are adjusted to produce the largest excess power, and in this model the power is maximized when the relaxation time is made equal to the inverse coherent transfer time). With these parameters, we obtain the results presented in Figure 4. This kind of model assumes that molecular  $D_2$  is embedded in a low Fermi level environment on the outer 10 microns of the cathode, and that the entire surface participates. This is consistent with excess heat results from the Szpak experiment, in which a roughly 10 micron thick co-deposited Pd layer on a copper substrate appears to lead to very similar levels of excess heat, but without the long lead time associated with the Fleischmann-Pons experiment.

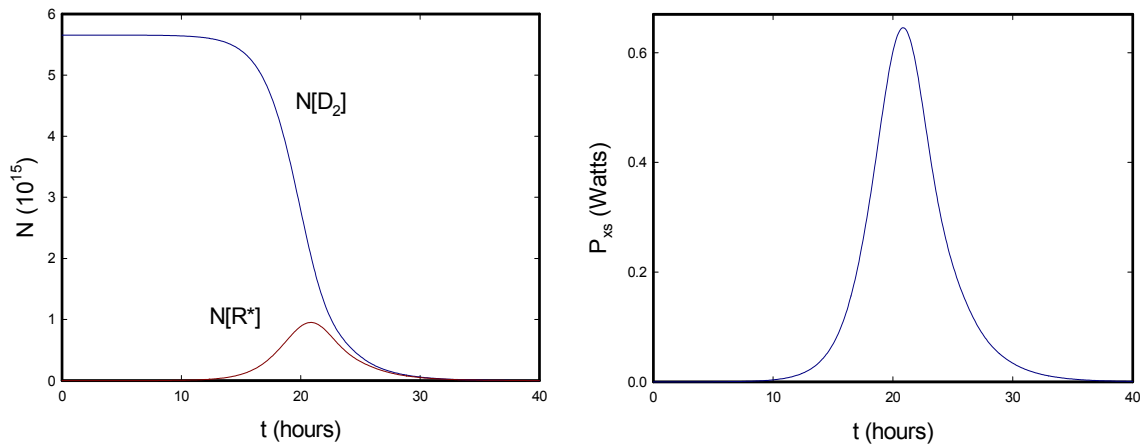


**Figure 4:** Results of a model simulation of an excess heat burst in a Fleischmann-Pons cell. On the left is plotted the  $D_2$  population in the coherent volume (which is a 10 micron thick layer around the surface of a 3 mm diameter Pd cathode 1 cm long), and also the excited state population in the receiver nuclei. On the right is shown the excess power as a function of time obtained from the energy loss of the excited state receiver nuclei. One sees that the model leads to simulation results comparable with experiment based on input parameters thought to be relevant to the experimental conditions.

## References

4. P. L. Hagelstein, "Unified phonon-coupled SU(N) models for anomalies in metal deuterides," *Proceedings of the 10<sup>th</sup> International Conference on Cold Fusion*, Cambridge, MA, Aug. 2003, p. 837.
5. P. L. Hagelstein, "Phonon-exchange models: Some new results," *Proceedings of the 11<sup>th</sup> International Conference on Cold Fusion*, Marseilles, France, Nov. 2004, p. 743.
6. P. L. Hagelstein, "Models for anomalies in condensed matter deuterides," *Proceedings of the 12<sup>th</sup> International Conference on Cold Fusion*, Yokohama, Japan, Dec. 2005, (in press).

## Modeling of the Yang-Koldomasov experiment

### RLE Group

Energy Production and Conversion Group

### Project Staff

Peter L. Hagelstein

### Introduction

A new kind of energy-producing device was announced at the 12<sup>th</sup> International Conference on Cold fusion by Hyunik Yang of Hanyang University in South Korea and his colleagues [1,2]. The device as presented is basically a closed loop around which oil is pumped, and forced through a plastic nozzle near Mach 1. In association with the oil flow, a discharge develops in the vicinity of the nozzle, which is readily seen by eye. It was claimed that the device can produce excess heat with a high energy gain (on the order of 500%). At the same conference and in previous conferences of the series, there have been presentations of modified Fleischmann-Pons experiments in which high power gain was observed. Mitchell Swartz described at last year's ANS conference his results with palladium cathodes and heavy water electrolysis the observation of energy gains up to 700%. The Israeli team has reported an energy gain (using a Pd foil electrolyzed in heavy water) in excess of 3000% using palladium cathodes. Tadahiko Mizuno described at ICCF12 an aqueous plasma-electrolysis experiment with a tungsten cathode in which a power gain in excess of 80000% was seen.

Consequently, a new claim of the observation of a 500% energy gain is not by itself out of line with what has been reported recently at the conferences. More significant is the claim that this kind of energy gain is 100% reproducible. Perhaps most interesting is that, if correct, it operates on a new principle as compared to other experiments being studied in the field. For example, in almost all of the other excess heat experiments, deuterium (and/or hydrogen) is loaded into a metal. In this new experiment, excess heat is claimed to be present with no metal. The only solids present in the vicinity of where the reactions take place are plastics, and one would not expect significant loading of the plastic with hydrogen or deuterium under the conditions of the experiment. Hence, if a similar kind of reaction is taking place, it may be occurring in a liquid rather than in a solid. This is interesting, and has attracted our interest.

### The cell

The simplest version of the cell looks something like what is shown in Figure 1. Oil flows in under pressure on the left, into the cell where it is forced through a nozzle inside the cell, and then exits on the right. Photographs of more complicated cell arrangements, in which metal discs are inserted upstream of the nozzle, are presented in the ICCF12 conference proceeding of S. Krivit. The basic claim associated with excess heat as presented at ICCF12 involves a comparison of the thermal power, as determined from thermal and pressure measurements taken on either side of the cell combined with measurements of the flow velocity, to the electrical power input to the pump. Measurements were performed in which the energy associated with the integrated temperature rise over a 15 minute run exceeded the electrical energy input over the same time by more than 400%.

When running, a discharge appears in the cell. In addition, cavitation bubbles are observed in the oil flow on the exit side of the cell.

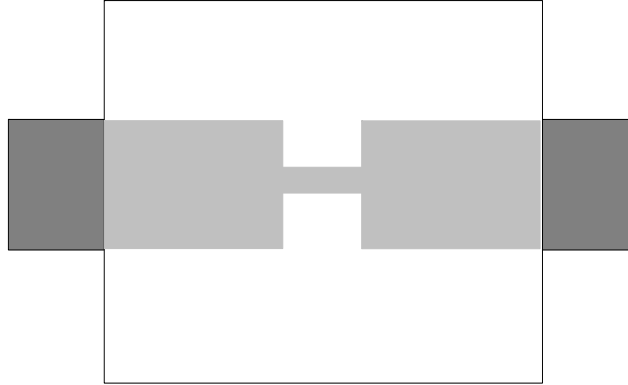


**Figure 1:** Schematic of a basic cell in the Yang-Koldomasov experiment. Oil flows in from the left in a metal pipe (indicated by dark grey), into a cylindrical plastic cell (light gray in white), through a nozzle inside the plastic cell (indicated by the restriction in light gray), and then out of the cell into an exit pipe.

### Theoretical notions

As presented at ICCF12, researchers working on the Yang-Koldomasov experiment proposed that the excess heat and related anomalies were due to aneutronic proton-boron fusion reactions. Such a proposal might be challenged since it is not obvious that sufficient kinetic energy is present anywhere in the experiment to overcome the associated Coulomb barrier. Some of the theoretical models that we have been developing for anomalies in metal deuterides may apply to this experiment. For example, the models which we have been developing have no requirement that the condensed matter phase be solid, and we consider the possibility that the Yang-Koldomasov experiment provides for such reactions in a liquid. According to our current thinking, the oil picks up charges from available surfaces in the vicinity of the nozzle and deposits them on downstream surfaces [3]. If the flow is sufficiently fast and if the oil has a low electrical conductivity, then the resulting charge imbalance can produce a discharge within the oil. Such an effect might be considered to be a liquid Van de Graaff effect. The temperatures produced within the discharge would be much too low to support any conventional nuclear reactions. However, it should be possible for chemical reactions to take place in the discharge. From our perspective, the primary function of the discharge in association with the anomalies is to produce a small amount of HD gas (along with much greater amounts of H<sub>2</sub> gas, as well as other chemical products, all of which are much less important) which is in solution in the oil.

The acceleration of the oil produced by pressure and nozzle in our view may be sufficient to produce nuclear excitation transfer reactions. In this case, excitation from the HD/<sup>3</sup>He system would be transferred to receiver nuclei in the oil. Given that the oil is essentially a hydrocarbon, the only nuclei present in significant quantities which appear promising as receiver nuclei are <sup>13</sup>C nuclei, which should permit neutron plus <sup>12</sup>C daughter excitations as required by the current version of the model. The Gamow factor is orders of magnitude larger for tunneling in HD as compared to tunneling in D<sub>2</sub>, so that the associated dynamics can be much faster. Once the excitation is transferred to the carbon nuclei, fast excitation transfer among the excited carbon nuclei supports the excitation (along with substantial angular momentum transfer from the acceleration field) until the fluid leaves the acceleration field. Once this occurs, fast excitation transfer can no longer be mediated by acceleration, and the excited nuclei would have to find decay channels. These would include x-ray and gamma-ray emission, as well as electron recoil decay channels. Fast electrons produced in this manner could be used for other applications [4].

### Modeling

It is possible to apply the excitation transfer model to this system under the assumptions described above. We consider the HD/<sup>3</sup>He system as one set of equivalent two-level systems,

and the  $^{13}\text{C}$  nuclei as another set of equivalent two-level systems. As long as the acceleration field is sufficiently strong, then there exist equivalent classical states in which  $n+^{12}\text{C}$  intermediate states with 20 or more units of relative angular momentum exist. In this case, we might model the excitation transfer using

$$H = \frac{\Delta E}{\hbar} \hat{S}_z^1 + \frac{\Delta E}{\hbar} \hat{S}_z^2 + \frac{V}{\hbar^2} e^{-G} \left( \hat{S}_+^1 \hat{S}_-^2 + \hat{S}_-^1 \hat{S}_+^2 \right)$$

Since the excitation transfer process is considered to take place over a very short time in which the associated fluid element remains in the acceleration field, we can make use of our Ehrenfest analysis without relaxation, and write

$$\begin{aligned} \frac{d}{dt} n_1 &= v_1 & \frac{d}{dt} n_2 &= v_2 \\ \frac{d}{dt} v_1 &= a & \frac{d}{dt} v_2 &= -a \end{aligned}$$

$$a = \frac{2V^2 e^{-2G}}{\hbar^2} \left\{ [N_1 - n_1][N_2 - n_2][n_2 - n_1] + n_1 n_2 [N_1 - n_1 - N_2 + n_2] + [N_1 - n_1] n_2 - [N_2 - n_2] n_1 \right\}$$

It is possible to develop a power series solution for  $n_2(t)$  valid for small  $t$ . Doing so allows us to obtain general analytic expressions for the reaction rate and excess power production. The series solution is

$$n_2(t) \approx \frac{n_{HD} n_{3He}}{(n_{HD} + n_{3He})} \left\{ (\Omega t)^2 + \frac{1}{3} (\Omega t)^4 + \frac{2}{45} (\Omega t)^6 + \dots \right\}$$

$$\Omega = \sqrt{(n_{HD} + n_{3He}) n_{13C}} V_{coh} \frac{V_{HD}}{\hbar} e^{-G}$$

Keeping only the leading order term leads to an estimate for the reaction rate given by

$$\Gamma = n_{HD} n_{3He} n_{13C} V_{coh}^3 \frac{V_{HD}^2}{\hbar^2} e^{-2G} t_0$$

Here,  $n_{HD}$ ,  $n_{3He}$ , and  $n_{13C}$ , are concentrations per cc of the nuclei involved in the excitation transfer process. The coherence volume associated with the acceleration field is  $V_{coh}$ , and  $t_0$  is the transit time through the acceleration field. The Gamow factor is approximately

$$e^{-G} = 1.6 \times 10^{-29} \quad [\text{tunneling in HD}]$$

We estimate for the coupling constant

$$V_{HD} = \sqrt{\frac{v_{nuc}}{v_{mol}}} U_0 = \sqrt{\frac{4\pi r_{nuc}^3}{3}} \sqrt{\frac{1}{4\pi d_{HD}^2 \Delta r}} U_0 = \sqrt{\frac{10^{-38}}{1.4 \times 10^{-24}}} 3 \text{ MeV} = 0.3 \text{ eV}$$

This is an equivalent model for what we used above for estimates in the case of  $D_2^AHe$  and the Fleischmann-Pons experiment.

**Results**

Two key features of the Yang-Koldomasov experiment emerge from this modeling. One is that  $^3He$  is required to support HD reactions at significant levels in this model. Given that very little  $^3He$  is present initially, and the reactions produce  $^3He$  as an ash, what is the associated dynamics. We may develop an evolution equation for the  $^3He$  inventory of the oil, assuming that helium is lost with a decay time  $\tau_{3He}$  and produced in the excitation transfer reactions

$$\frac{d}{dt} N_{3He} + \frac{N_{3He}}{\tau_{3He}} = \left[ n_{HD} n_{13C} V_{coh}^3 \frac{V_{HD}^2}{\hbar^2} e^{-2G} t_0 \right] \frac{N_{3He}}{V_{oil}}$$

We see that  $^3He$  builds up exponentially in this model as long as the gain is greater than the loss

$$\frac{1}{V_{oil}} n_{HD} n_{13C} V_{coh}^3 \frac{V_{HD}^2}{\hbar^2} e^{-2G} t_0 > \frac{1}{\tau_{3He}}$$

The rate of growth for  $^3He$  in this model has a strong dependence on the coherence volume assumed. We illustrate results for the growth rate in Figure 2 estimated using representative numbers: 1 mm nozzle radius r, 35 liters of oil, and a flow velocity of 500 m/sec. The resulting model growth rates are thought to be in the right range for the Yang-Koldomasov experiment, which operates using oil with deuterium present at natural isotopic abundance.

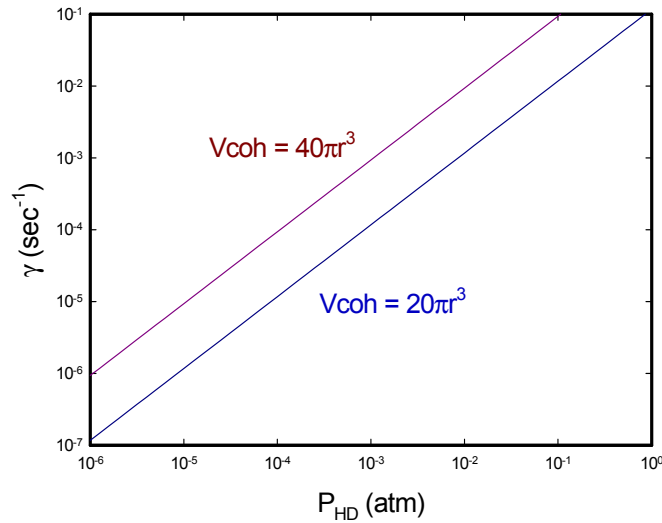


**Figure 2:** Model result for  $^3He$  growth rate in the Yang-Koldomasov as a function of HD partial pressure.

The other feature of the experiment that is of interest is the associated power level. Results from the excitation transfer model are shown in Figure 3 (calculated using the differential equation and not the parabolic approximation). According to the model, significant excess power (given that implementations run at power levels on the order of 1 kW or above) is obtained only when the  $^3He$  levels have built up to about 1 atmosphere partial pressure.

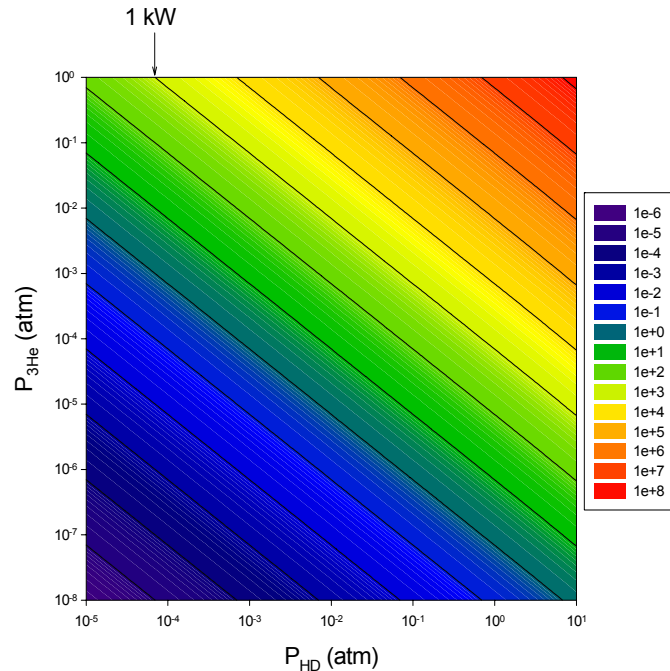


**Figure 3:** Model result power production in the Yang-Koldomasov as a function of HD partial pressure and  $^3\text{He}$  partial pressure. Calculations are for similar parameters as for Figure 2, with the coherence volume taken to be  $20\pi r^3$ .

## Discussion

If the Yang-Koldomasov experiment is correct, then according to our ideas of how it works, it would be very closely related to the Fleischmann-Pons experiment. This new experiment would be perhaps more interesting scientifically since it is simpler, since there is no second step of energy relaxation to the lattice, which hides the reaction process in the Fleischmann-Pons experiment. In this experiment, only the excitation transfer step occurs (followed by a decay of energetic reaction products), which makes it much simpler, and hence easier to analyze.

We are at present hosting a confirmation test of a Yang-Koldomasov experiment in our lab. Our hope is to be able to run the experiment under conditions obtain previously where positive results were obtained, and attempt a confirmation of energy gain, fast electron generation, and if possible  $^3\text{He}$  production.

## References

7. S. B. Krivit, "Introduction to a new method to initiate cold fusion/condensed matter nuclear reactions," *Proceedings of the 12<sup>th</sup> International Conference on Cold Fusion*, Yokohama, Japan, Dec. 2005, (in press).
8. V. I. Vysostskii, et al, presented at the *12<sup>th</sup> International Conference on Cold Fusion*, Yokohama, Japan, Dec. 2005.
9. I. Koszman and J. Gavis, "Development of charge in low-conductivity liquids flowing past surfaces," *Chem. Eng. Sci.* **17** 1013 (1962).
10. H. Yang and A. I. Koldomasov, Apparatus for generating hydrogen gas, Korean Patent WO/041715 A1 (2004).